NUCL SCI TECH (2021) 32:120
https://doi.org/10.1007/s41365-021-00965-0

Performance of a plastic scintillation fiber dosimeter based on different photoelectric devices

Yue Yang[1] · Cui-Ping Yang[1,2] · Jie Xin[1,3] · Hai-Feng Chen[1] · Zhong-Xu Xing[1] · Wei-Wei Qu[1,4] · Liang Hu[1,4] · Xin-Jian Chen[1] · Ren-Sheng Wang[1,4]

Received: 30 August 2021 / Revised: 8 October 2021 / Accepted: 14 October 2021 / Published online: 16 November 2021

Abstract The photoelectric device of a scintillation dosimeter converts photons produced by radiation into an electrical signal. Its features directly determine the overall performance of the dosimeter. For a plastic scintillation fiber dosimeter (PSFD) with a current readout mode, systematic studies of the stability and light-dose response were performed for the photomultiplier tube (PMT), silicon photomultiplier (SiPM), avalanche photodiode (APD), and photodiode (PD). The temperature stability, long-term stability, repeatability, signal-to-noise ratio (SNR), and current dose response of the PSFD with the abovementioned photoelectric devices were studied using a pulsed LED light source and the Small Animal Radiation Therapy platform. An exponential relationship between the dark/net current and temperature was obtained for all the devices. It is shown that the APD is the most sensitive device to temperature, with a current dependence on temperature reaching $6.5\%\,^{\circ}\mathrm{C}^{-1}$ at room temperature, whereas for the other devices this dependence is always $<0.6\%\,^{\circ}\mathrm{C}^{-1}$. In terms of long-term stability, the net current of PD can change by up to 4% when working continuously for 8 h and 2% when working intermittently for 32 h, whereas for the other devices, the changes are all <1%. For the dose response, the PMT and SiPM exhibit excellent linear responses and SNRs within the range of 0.1–60 Gy/min. For the PSFD with a current readout mode, the performance of the PMT and SiPM is concluded to be better than that of the other devices in the study. In particular, the SiPM, which has a compact size, low bias voltage, and antimagnetic interference, has great advantages for further applications.

Keywords Photoelectric device · Plastic scintillation fiber dosimeter (PSFD) · Current readout · Dose response

This work was supported by the China Postdoctoral Science Foundation (No. 2017M621818), the National Key Research and Development Project (Nos. 2017YFF0206205 and 2016YFB0501303), the National Natural Science Foundation of China (Nos. 51873137 and 11705123), and the Project of the State Key Laboratory of Radiation Medicine and Protection, Soochow University (No. GZN1201801).

✉ Wei-Wei Qu
wwqu@suda.edu.cn

✉ Liang Hu
huliang@suda.edu.cn

✉ Ren-Sheng Wang
wrs16@suda.edu.cn

1 State Key Laboratory of Radiation Medicine and Protection, School of Radiation Medicine and Protection, Soochow University, Suzhou 215123, China

2 Renji Hospital, Affiliated with the Shanghai Jiao Tong University School of Medicine, Shanghai 200127, China

3 Shanghai Ninth People's Hospital, Affiliated with the Shanghai Jiao Tong University School of Medicine, Shanghai 200127, China

4 Collaborative Innovation Center of Radiological Medicine of Jiangsu Higher Education Institutions, Suzhou 215123, China

1 Introduction

In vivo dosimetry (IVD) is one of the most direct methods for quality assurance during radiation therapy and is now widely recommended. IVD can provide a real-time dose rate of a reference site or the dose rate distribution of a certain tissue in the radiation field, which can be used to assess the differences between the planned and delivered dose [1–3]. An effective dose imaging system or point dosimeter is key to IVD. Dose imaging systems, such as electronic portal imaging devices [4], positron emission tomography, and single photon emission computed tomography in particle therapy [5], are the highest performing systems for IVD, but they also require advanced technology and imagining support and are still not fully implemented or explored. In contrast, point dosimeters are widely used in IVD because of their simple structure and intuitive measurement results. Several types of point dosimeters have been explored in IVD; these include as diode dosimeters [6], metal oxide semiconductor field effect transistors [7], new semiconductor dosimeters [8], and plastic scintillation fiber dosimeters (PSFDs) [9–14]. With the advantages of good tissue equivalence, radiation resistance, small size, and highly reliable accuracy, the PSFD is one of the most promising point dosimeters used in IVD [15].

For the PSFD, the absorbed dose of the scintillation fiber can be obtained by measuring its light yield using a photoelectric device. Within a certain dose rate, the operation current of the photoelectric device is linearly proportional to the intensity of the measured light. Therefore, by measuring the operating current of the photoelectric device, the absorbed dose of the scintillation fiber can be measured; this is also called the current mode of the PSFD. Normally, the operation current or the integral charge of a photoelectric device can be measured by an electrometer or a picoammeter. The relationship between the current of the photoelectric device and the dose rate is called the current dose response of the PSFD. So far, the photoelectric devices used in PSFDs include photomultiplier tubes (PMTs) [9], silicon photomultipliers (SiPMs) [10, 11], avalanche photodiodes (APDs) [12], and photodiodes (PDs) [13, 14]. For a working photoelectric device, the operation current consists of the dark current and the net current, both of which are important for accurate measurement results. This type of stability includes not only stability against environmental interference but also the stability of the device itself during long-term operation. A device with worse stability requires more repetitive calibration, which limits its applications.

Using a plastic scintillation fiber with a diameter of 1 mm and a length of 10 mm, and a white fiber with a length of 10 m, Boivin et al. [16] systematically studied the dose response characteristics of PSFDs based on different photoelectric devices such as PMTs, APDs, PDs, and CCD cameras. In Boivin et al.'s work, the energy dependence, signal-to-noise ratio (SNR), and linearity were studied. However, the stability of PSFDs has not been systematically investigated, and this is a necessary step before their widespread use. In addition, as a new type of photoelectric device, the SiPM has the advantages of small size and high gain, which is comparable with PMTs and an optimal choice for PSFDs. Therefore, based on the same testing device and method, in this study we systematically tested the stability and dose response of the above four photoelectric devices, namely, PMTs, SiPMs, APDs, and PDs. The structure of the PSFD is described in Sect. 2. The method and results of the stability test of the dosimeter and the dose response and SNR are presented in Sects. 3 and 4, respectively. Finally, the conclusions are presented in the last section.

2 Dosimeter structure

Unlike the direct collection of electrons and ions in an ionization chamber, the dose signal of a PSFD requires light transmission. A schematic of a PSFD is shown in Fig. 1a. The PSFD is mainly divided into four parts: plastic scintillation fiber, white transmission fiber, a photoelectric device, and a readout circuit board. The plastic scintillation fiber used in this study was BCF-10 (Saint Gobain Co.) with a diameter of 0.5 mm and a length of 3 mm. The scintillation fiber converts the energy deposited by radiation into photons, which are proportional to the deposited energy. The transmission white fiber adopted was GH-4001 (Mitsubishi Co.) with an inner core diameter of 1.0 mm and a length of 2.5 m, which transmits the photons generated in the scintillation fiber for further measurement. The coupling between the scintillation fiber and white fiber was polished with fiber grinding paper, as shown in Fig. 1b. The ends of these two fibers were coupled by EJ550 optical silicone grease. Two layers of WOLIDA E329530 black heat shrinkable tubes were used for fixing and shielding the light.

The photoelectric devices used in this study were all manufactured by Hamamatsu. The PMT, SiPM, APD, and PD models were H3164-10, S13360-3025CS, S8664-1010, and S9032-02, respectively. The photoelectric device and the current readout circuit board were placed into a $7 \times 7 \times 7\mathrm{cm}^3$ aluminum box to achieve light-proof and electromagnetic shielding. Meanwhile, a homemade temperature-control device was attached to the outside of the aluminum box to achieve constant temperature control with an accuracy of $\pm 0.1\,^{\circ}\mathrm{C}$. As shown in Fig. 1a, the homemade temperature-control device included a semiconductor refrigeration chip with a cooling power of 30 W, a resistance heating plate with a heating power of 6 W, and two sets of temperature probes and constant-temperature controllers for cooling or heating separately. The semiconductor refrigeration chip was in external contact with the aluminum box through a thermally conductive silica gel. Temperature sensor 1 for cooling was covered by thermal

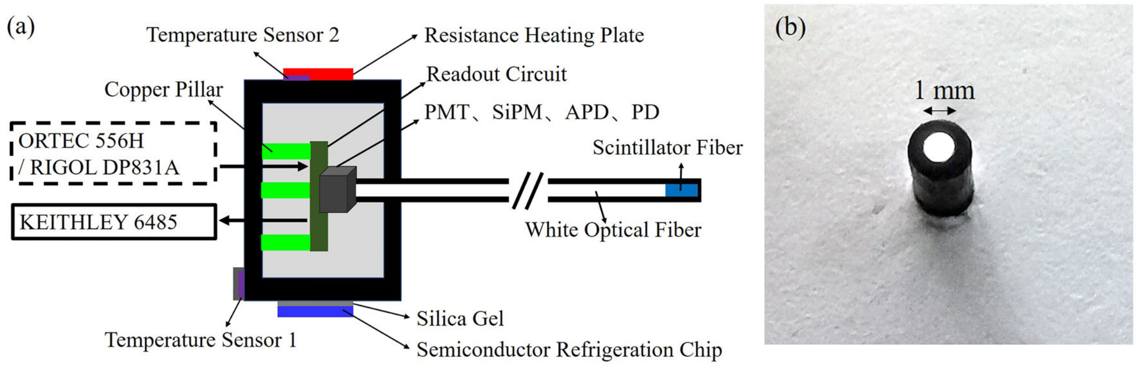

Fig. 1 (Color online) **a** Schematic of a fiber dosimeter. **b** Photograph of the polished end face of a white optical fiber

insulation cotton and was in direct external contact with the aluminum box. The resistance heating plate itself included temperature sensor 2. The circuit board on which the photoelectric device was located was copper-clad on one side. For heat conduction, the copper-clad surface was connected to the aluminum box through three copper pillars with diameters of 3 mm and lengths of 10 mm. To ensure that thermal balance was reached, each time the temperature was adjusted, the measurement was taken after 30 min.

The bias voltages of the PMT, SiPM, and APD were all provided by an ORTEC 566H power module, and these were set to 1250, 58, and 380 V, respectively. Because the bias voltage of the PD is only 1 V, for accurate repeat setting, a RIGOL DP831A linear DC power was used. The current of the device was measured using a Keithley 6485 picoammeter. For the SiPM, APD, and PD, the bias circuit was grounded through the picoammeter, so that the operation current could be read directly by a picoammeter. For the PMT, the cathode was biased with a negative high voltage, and the picoammeter was placed between the anode and the ground. The resolution of the picoammeter can achieve 10 fA, which is sufficient for the current measurement of the PD with the lowest operating current. The current integration time was set as 1 s.

3 Environmental stability

For packaged solid-state devices, the most influential factors are temperature and long-term operation, which will be studied in this section. Long-term stable radiation sources are difficult to fabricate. Therefore, an LED pulse light source was used for stability testing. The wavelength peak of the LED was 465 nm (blue light). A precision pulse generator was used to produce a rectangular pulse to excite the LED. By adjusting the frequency, duty cycle, and amplitude of the excitation pulse, the LED pulsed light can be equivalent to the fluorescence produced by the plastic scintillation fiber at a certain radiation dose rate. The details can be found in [17].

3.1 Temperature stability

With the temperature-control device introduced in Sect. 2, the temperature of the aluminum box can be continuously controlled from 15 °C to 33 °C. After each temperature adjustment, 30 min was used for stabilization to ensure that the photoelectric device and the aluminum box reached thermal equilibrium. For each device under each temperature condition, the dark current and net current were measured multiple times. The average of multiple measurements was taken as the measured value, and the error bars are the corresponding standard deviations.

Dark current (I_{Dark}) refers to the operating current of the device without any light. The response of I_{Dark} to the temperature for the four devices is shown in Fig. 2a. The black solid square represents the PMT, the red hollow square represents the SiPM, the blue solid triangle represents the APD, and the pink hollow triangle represents the PD. To facilitate comparison, I_{Dark} of the PD in Fig. 2a has been multiplied by 10^3. The mechanisms of these four devices are different, and the dark current spans five orders of magnitude from picoamperes to hundreds of nanoamperes; it can be seen that the dark current increases approximately exponentially with the increase in temperature from 15 ° C to 35 ° C. To quantitatively describe the dependence of I_{Dark} on temperature, the exponential formula

$$I = \exp[kT + b] \tag{1}$$

was used to fit the data, and the slope k in the fitting results are shown in Fig. 2a. k characterizes the temperature dependence of I_{Dark}. The larger the value of k, the more sensitive I_{Dark} is to the temperature. It can be observed from Fig. 2a that I_{Dark} of the PMT is the most sensitive to temperature, followed by the PD and SiPM, and the relatively most stable device is the APD. The error bars are

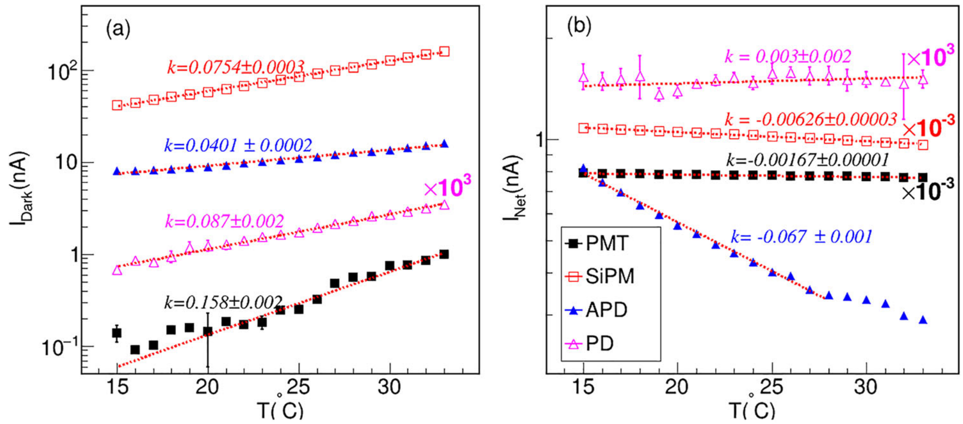

Fig. 2 (Color online) Change of **a** dark current and **b** net current of photoelectric devices as a function of temperature

smaller than the symbols themselves; therefore, they are not visible.

The net current (I_{Net}) is the operation current subtracted from the related I_{Dark}. Figure 2b shows the variation of the I_{Net} with temperature for these devices when the equivalent dose rate of 6 Gy/min was furnished by the LED. Similarly, for convenience of comparison, I_{Net} of the PD in the figure is multiplied by 10^3, while I_{Net} of the PMT and SiPM is multiplied by 10^{-3}. It can be seen that the I_{Net} values of these four devices also change with an exponential function of temperature. Therefore, Eq. 1 was also used to fit the measurement values again, and the slope k is also shown in Fig. 2b. For the APD, when the temperature was higher than 28 $^\circ$ C, the dependence of I_{Net} on the temperature deviates from the exponential relationship; consequently, it was not considered in the fitting.

It can be seen from the test measurement that, for devices with signal amplification, I_{Net} decreases with increasing temperature, which means that higher temperatures will reduce their amplification gain. This is mainly because the quantum conversion efficiency of the photocathode decreases with increasing temperature; therefore, the overall gain decreases [18, 19]. For the SiPM and APD, because the breakdown voltage V_{BD} of the device increases with temperature, this leads to a decrease in their gain [20, 21]. Nevertheless, the stability performance of the PMT, SiPM, and PD are similar, and the dependence of I_{Net} on temperature is $<(1-e^{-0.006}) = 0.6\%\,^\circ\mathrm{C}^{-1}$. The dependence of the APD on temperature was the largest, being $\sim\ (1-e^{-0.067}) = 6.5\%\,^\circ\mathrm{C}^{-1}$.

3.2 Long-term stability

Given the needs of practical applications, the long-term stability test includes two aspects: continuous stability and repeatability stability. Therefore, a study of the changes in I_{Net} with time was performed under the conditions of continuous working for 8 h and intermittent working for 32 h. During the measurement, the temperature of the device was controlled within a range of $20\,^\circ\mathrm{C} \pm 0.1\,^\circ\mathrm{C}$. The continuous stability test records I_{Net} at 0, 0.1, 0.25, 0.75, 1.75, 2.75, 4, 6, and 8 h, respectively. The repeatability stability test records I_{Net} at 0.1, 0.5, 1, 2, 3, 6, 18, 24, and 32 h, respectively. For the repeatability test, after each measurement, the bias voltage was reduced to 0 V and disconnected. For each device, the reference current (I_0) was measured for the first time. According to

$$R_{current} = (I_i - I_0)/I_0, \quad (2)$$

the current change rate ($R_{current}$) of the ith measured current (I_i) was calculated, and the results are shown in Fig. 3. The identification symbols of the different devices are the same as those defined in Fig. 2. Figure 3a shows the change of $R_{current}$ under the continuous working mode. The two horizontal black dotted lines in the figure represent $\pm 0.5\%$. It can be seen that $R_{current}$ of the PD is the largest and can reach up to 4%, whereas all the other devices have values of $<0.5\%$. In particular, the PMT is the most stable, with $R_{current} < 0.2\%$. Figure 3b shows the change of $R_{current}$ under intermittent work for 32 h. The two dashed black lines represent $\pm 1.0\%$. Similarly, $R_{current}$ of the PD is the largest, being up to 2%, whereas all the other devices have values of $<1\%$, with the SiPM being the most stable, with $R_{current} < 0.5\%$.

4 Dose response

The PSFD can measure the dose rate in real time, and the total dose can be obtained by integrating the dose rate. A practical dosimeter requires a good SNR at a low dose rate and a wide linear response range. Therefore, the dose response of different photoelectric devices was studied, including the linear dynamic range and SNR.

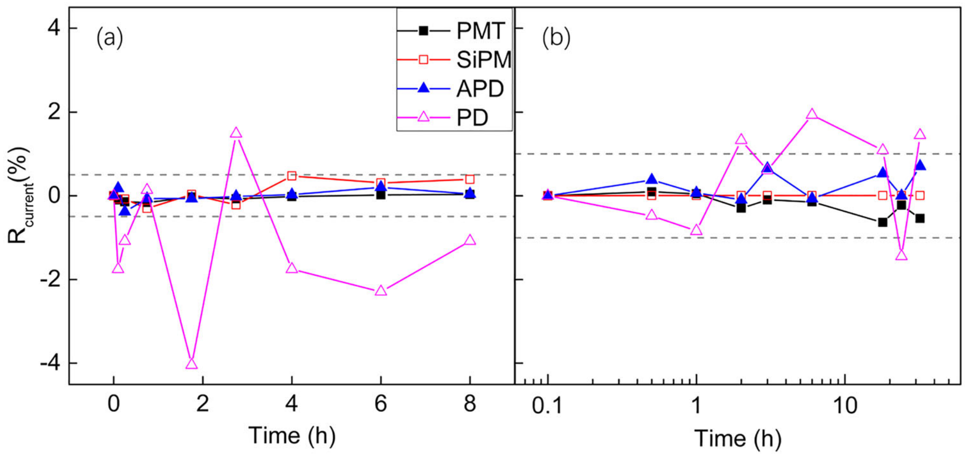

Fig. 3 (Color online) Change in the operation current as a function of time in **a** continuous mode for 8 h and **b** discontinuous mode for 32 h

4.1 Linear response range

The linear response range of the dose rate is an important indicator for a dosimeter. A wide linear response range can greatly simplify calibration in the application. The dose rate range of the Small Animal Radiation Therapy (SmART+) platform used in this study was 0.086–4.5 Gy/min, and the maximum voltage of SmART+ is 225 kV. To extend the test range of the dose rate, the following two methods were used: (1) The effective length of the scintillation fiber was increased, thereby increasing its equivalent dose rate, so that the calibrated range of dose rate can reach 0.333–14.85 Gy/min; (2) based on the scaled LED pulse light source [22], the dose rate range can reach 10.15–60.15 Gy/min.

Figure 4 shows the relationship between I_{Net} and the dose rate for four kinds of devices. A linear fitting function was used to fit the measured value, as shown in Fig. 4.

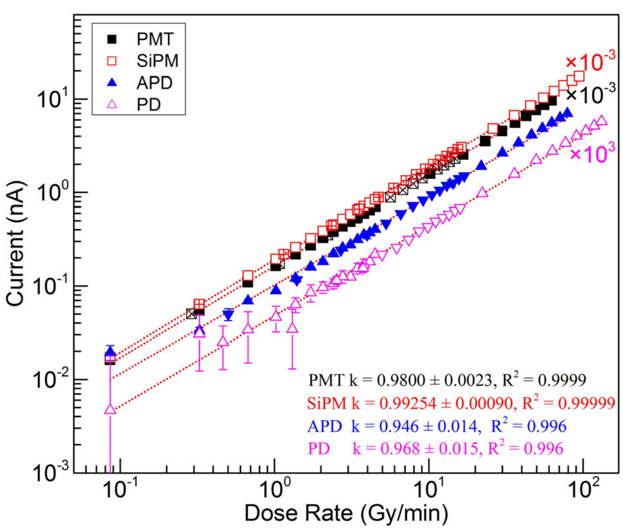

Fig. 4 (Color online) Relationship between the dose rate and the operation current of the PMT, SiPM, APD, and PD

Each point was averaged over those three measured values, and the standard deviation was taken as the error. After the beam was turned on and the tube voltage display was allowed to stabilize, 10 different dose rates were measured. It can be seen from Fig. 4 that both the PMT and SiPM exhibit excellent linear responses in a wide dose rate range from 0.1 to 60 Gy/min. The APD exhibits a linear response to the dose rate in the range from 0.4 to 60 Gy/min, but the linear correlation coefficient R^2 is lower than those of the PMT and SiPM. There is no gain to the optical signal for the PD, so that I_{Net} is only tens to hundreds of femtoamperes with a large fluctuation on the picoammeter. Based on the measurement results, the PD was considered to have a good linear response under the conditions of 0.2–60 Gy/min.

It can be seen from these measurements that all the devices have good linearity at high dose rates, which means that in high-dose-rate applications, low-cost, high-stability devices should be selected (e.g., SiPMs). However, at low dose rates, it is necessary to amplify the optical signal, and SiPMs and PMTs are better choices.

4.2 SNR

The SNR can be used to evaluate the sensitivity of the dosimeter. Here, the SNR is an overall assessment of sensitivity—not only being the ratio of net current to dark current but also a measure of the stability of the net current and dark current. The definition [23] is given as

$$SNR = \mu_s / \mu_0, \tag{3}$$

where μ_0 and μ_s represent the average value and standard deviation of multiple measurements, respectively. A higher SNR value indicates a higher sensitivity of the device under a given radiation field with a fixed dose rate. The SNRs of the devices at different dose rates are summarized in Fig. 5. According to the Rose standard, the target value

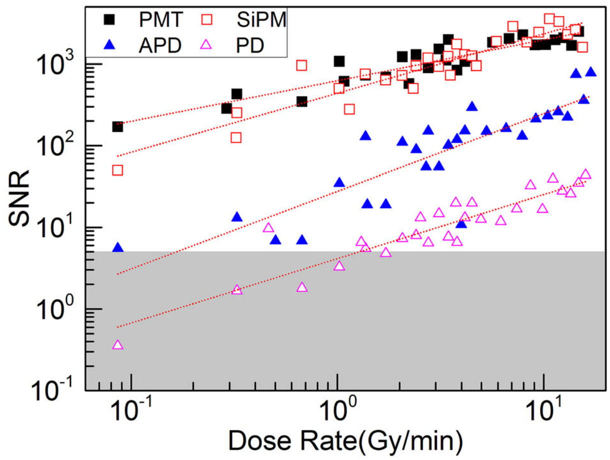

Fig. 5 (Color online) SNRs of the PMT, SiPM, APD, and PD at different dose rates

is generally considered to be correctly detected when $SNR > 5$ [24].

It can be observed from Fig. 5 that the SNR of the PMT and SiPM are quite similar. Both the PMT and SiPM exhibit excellent performance even at a dose rate of 0.1 Gy/min, with SNR values of 170 and 50, respectively. Then, the SNR increases as the dose rate increases, and it tends to be the same when the dose rate is >2 Gy/min for the PMT and SiPM. This is mainly because the dark current is the largest contributor to the SNR at low dose rates. Then, as the dose rate increases, the fluctuation of the dark current did not change, but the net current increased stably. For the APD, the SNR is slightly greater than 5 at the lowest dose rate of 0.1 Gy/min. Obviously, the accuracy may be disturbed by noise at 0.1 Gy/min. The PD had the lowest SNR value, being <5 until the dose rate was >2 Gy/min.

5 Summary

An LED pulse light source and the SmART+ platform were used to systematically study the environmental stability and dose rate response performance of PSFDs with four different photoelectric devices (PMT, SiPM, APD, and PD), which provides a reference for selecting the photoelectric device.

Based on the results, the following conclusions can be made: (1) In terms of temperature stability, I_{Net} of the APD is most susceptible to temperature, with a current dependence on temperature of up to 6.5% $^{\circ}\mathrm{C}^{-1}$, whereas the other devices all had values of <0.6% $^{\circ}\mathrm{C}^{-1}$. (2) For continuous working stability, the maximum change of the PD can reach 4%, whereas the other devices all had values of <1%. (3) For the dose rate response, in the range of 0.1–60 Gy/min, both the PMT and the SiPM exhibited excellent linear responses and SNRs. A comprehensive comparison of these four photoelectric devices was made, and it was concluded that the SiPM and PMT are more suitable for scintillation fiber dosimeters based on operation current readout. In particular, the SiPM has a small size, is less affected by magnetic fields, has a low working bias voltage, and thus has great advantages in terms of convenience, such as portability.

Author contributions All authors contributed to the study conception and design. Material preparation, data collection, and analysis were performed by Yue Yang, Cui-Ping Yang, and Ren-Sheng Wang. The first draft of the manuscript was written by Ren-Sheng Wang, and all authors commented on previous versions of the manuscript. All authors read and approved the final manuscript.

References

1. M. Essers, B. Mijnheer, In vivo dosimetry during external photon beam radiotherapy. Int. J. Radiat. Oncol. Biol. Phys. **43**(2), 245–259 (1999). https://doi.org/10.1016/S0360-3016(98)00341-1
2. A.S. Beddar, Plastic scintillation dosimetry and its application to radiotherapy. Radiat. Meas. **41**, S124–S133 (2006). https://doi.org/10.1016/j.radmeas.2007.01.002
3. G.P. Fonseca, J.G. Johansen, R.L. Smith et al., In vivo dosimetry in brachytherapy: requirements and future directions for research, development, and clinical practice. Phys. Imaging Radiat. Oncol. **16**, 1–11 (2020). https://doi.org/10.1016/j.phro.2020.09.002
4. S. Celi, E. Costa, C. Wessels et al., EPID based in vivo dosimetry system: clinical experience and results. J. Appl. Clin. Med. Phys. **17**, 262–276 (2016). https://doi.org/10.1120/jacmp.v17i3.6070
5. K. Parodi, J.C. Polf, In-vivo range verification in particle therapy. Med. Phys. **62**, L41 (2017). https://doi.org/10.1002/mp.12960
6. Diode in Vivo Dosimetry for Patients Receiving External Beam Radiation Therapy. AAPM REPORT NO. 87 https://doi.org/10.37206/881
7. R. Consorti, A. Petrucci, F. Fortunato et al., In vivo dosimetry with MOSFETs: dosimetric characterization and first clinical results in intraoperative radiotherapy. Int. J. Radiat. Oncol. Biol. Phys. **63**(3), 952–960 (2005). https://doi.org/10.1016/j.ijrobp.2005.02.049
8. L. Chai, L. Chen, C.P. Yang et al., Evaluation of CdZnTe spectrometer performance in measuring energy spectra during interventional radiology procedure. Nucl. Sci. Tech. **30**, 137 (2019). https://doi.org/10.1007/s41365-019-0661-8
9. A.S. Beddar, T.R. Mackie, F.H. Attix, Water-equivalent plastic scintillation detectors for high-energy beam dosimetry: II. Properties and measurements. Phys. Med. Biol. **37**(10), 1901 (1992). https://doi.org/10.1088/0031-9155/37/10/007
10. A. Berra, V. Conti, D. Lietti et al., A SiPM based real time dosimeter for radiotherapic beams. Nucl. Instrum. Methods Phys. Res. A **773**, 72–80 (2015). https://doi.org/10.1016/j.nima.2014.11.001
11. A. Berra, A. Ferri, C. Novati et al., Single and multichannel scintillating fiber dosimeter for radiotherapic beams with SiPM readout. Nucl. Instrum. Methods Phys. Res. A **838**, 1–11 (2016). https://doi.org/10.1016/j.nima.2016.08.068
12. M. De Gerone, S. Dussoni, F. Gatti et al., Development and characterization of scintillating fiber-APD-based detector. Nucl.

Instrum. Methods Phys. Res. A **610**, 218–221 (2009). https://doi.org/10.1016/j.nima.2009.05.159
13. F. Rego, L. Peralta, M. da Concei Abreu, A Scintillating Fiber Dosimeter for Radiology and Brachytherapy with photodiode readout. arXiv:1109.6545v1(2011)
14. F. Therriault-Proulx, T.M. Briere, F. Mourtada et al., A phantom study of an in vivo dosimetry system using plastic scintillation detectors for real-time verification of ^{1}92Ir HDR brachytherapy. Med. Phys. **38**, 2542–2551 (2011). https://doi.org/10.1118/1.3572229
15. S. O'Keeffe, D. McCarthy, P. Woulfe et al., A review of recent advances in optical fibre sensors for in vivo dosimetry during radiotherapy. Med. Phys. **88**, 1050 (2015). https://doi.org/10.1259/bjr.20140702
16. J. Boivin, S. Beddar, M. Guillemette et al., Systematic evaluation of photodetector performance for plastic scintillation dosimetry. Med. Phys. **42**, 6211–20 (2015). https://doi.org/10.1118/1.4931979
17. C.P. Yang, J. Xin, D.D. Zhou et al., Development of a SiPM-based practical plastic scintillation fiber dosimeter. Nucl. Tech. **42**, 100402 (2019). https://doi.org/10.11889/j.0253-3219.2019.hjs.42.100402 (**in Chinese**)
18. H.M. Araujo, A. Bewick, D. Davidge et al., Low-temperature study of 35 photomultiplier tubes for the ZEPLIN III experiment. Nucl. Instrum. Methods Phys. Res. A **521**, 407–415 (2004). https://doi.org/10.1016/j.nima.2003.10.094
19. A. Lyashenko, T. Nguyen, A. Snyder et al., Measurement of the absolute Quantum Efficiency of Hamamatsu model R11410-10 photomultiplier tubes at low temperatures down to liquid xenon boiling point. J. Instrum. **9**, P11021 (2014). https://doi.org/10.1088/1748-0221/9/11/P11021
20. A.N. Otte, D. Garcia, T. Nguyen et al., Characterization of three high efficiency and blue sensitive silicon photomultipliers. Nucl. Instrum. Methods Phys. Res. A **846**, 106–125 (2017). https://doi.org/10.1016/j.nima.2016.09.053
21. L. Yang, S. Dzhosyuk, J.M. Gabrielse et al., Performance of a large-area avalanche photodiode at low temperature for scintillation detection. Nucl. Instrum. Methods Phys. Res. A **508**, 388–393 (2003). https://doi.org/10.1016/S0168-9002(03)01665-6
22. Y. Yin, J. Lambert, D.R. McKenzie et al., Real-time monitoring and diagnosis of scintillation dosimeters using an ultraviolet light emitting diode. Phys. Med. Biol. **53**, 2303 (2008). https://doi.org/10.1088/0031-9155/53/9/007
23. H.M.L. Rosales, P. Duguay-Drouin, L. Archambault et al., Optimization of a multipoint plastic scintillator dosimeter for high dose rate brachytherapy. Med. Phys. **46**, 2412–2421 (2019). https://doi.org/10.1002/mp.13498
24. J.A. Seibert, *The Essential Physics of Medical Imaging* (Williams & Wilkins, Philadelphia, 2013)